INTERNATIONAL JOURNAL OF REFRIGERATION 55 (2015) 201–211

Available online at www.sciencedirect.com

ScienceDirect

journal homepage: www.elsevier.com/locate/ijrefrig

Investigation of an experimental ejector refrigeration machine operating with refrigerant R245fa at design and off-design working conditions. Part 1. Theoretical analysis

K.O. Shestopalov [a,b,*], B.J. Huang [a], V.O. Petrenko [a,b], O.S. Volovyk [a]

[a] New Energy Center, Department of Mechanical Engineering, National Taiwan University, Taipei 106, Taiwan
[b] Odessa State Academy of Refrigeration, Ejector Refrigeration Technologies Center, 1/3, Dvoryanskaya St., 65082 Odessa, Ukraine

ARTICLE INFO

Article history:
Received 18 July 2014
Received in revised form
29 December 2014
Accepted 27 January 2015
Available online 5 March 2015

Keywords:
Ejector
Ejector refrigeration machine
R245fa
Performance characteristics
1-D analysis

ABSTRACT

The ejector refrigeration machine (ERM) offers several advantages over other heat-driven refrigeration machine, including simplicity in design and operation, high reliability and low installation cost, which enable its wide application in the production of cooling. In this paper the theoretical analysis of ejector design and ejector refrigeration cycle performance is presented. It is shown that ERM performance characteristics depend strongly on the operating conditions, the efficiency of the ejector used, and the thermodynamic properties of the refrigerant used. A 1-D model for the prediction of the entrainment ratio ω, and an optimal design for ejectors with cylindrical and conical-cylindrical mixing chambers are presented in this paper. In order to increase ERM performance values, it is necessary first of all to improve the performance of the ejector.

Une étude du fonctionnement d'un système frigorifique expérimental à éjecteur avec le frigorigène R245fa aux conditions de travail de conception et hors-conception. 1ère partie- Analyse théorique

Mots-clés : Ejecteur ; Machine frigorifique à éjecteur ; R245fa ; Caractéristiques de performance ; Analyse unidimensionnelle

* *Corresponding author*. New Energy Center, Department of Mechanical Engineering, National Taiwan University, Taipei 106, Taiwan. Tel.: +886 2 23634790.
E-mail address: konalex2@yandex.ru (K.O. Shestopalov).
http://dx.doi.org/10.1016/j.ijrefrig.2015.01.016
0140-7007/

Nomenclature

A	area, mm^2
a	sonic velocity, m s^{-1}
C	ejector compression ratio
c_p	constant pressure specific heat, kJ kg^{-1} K^{-1}
COP	coefficient of performance
CCMC	conical-cylindrical mixing chamber
CMC	cylindrical mixing chamber
E	ejector expansion ratio
ERM	ejector refrigeration machine
h	specific enthalpy, kJ kg^{-1}
M	molecular weight, kg $kmol^{-1}$
$\dot{m}$	mass flow rate, kg s^{-1}
P	pressure, bar
Q	heat flow, kW
q	specific heat, kJ kg^{-1}
R	universal gas constant, J K^{-1} mol^{-1}
r	latent heat, kJ kg^{-1};
s	specific entropy, kJ kg^{-1} K^{-1}
T	temperature, C or K
V	gas velocity, m s^{-1}
v	specific volume, m^3 kg^{-1}
$\dot{W}$	power, W

Greek letters

$\alpha, \beta, \sigma, \phi$	ejector area ratios
γ	ratio of specific heats
$\varepsilon, \lambda, \Pi$	gas-dynamic functions
η	coefficient of efficiency
Θ	dimensionless temperature
ρ	density, kg m^{-3}
φ	velocity coefficient
ψ	converging angle at mixing chamber entrance
ω	entrainment ratio

Subscripts

c	condenser
x	critical
e	evaporator
fp	feed pump
g	generator
m	mixture
max	maximum
mech	mechanical
opt	optimum
p	primary
s	secondary
suc	suction
t	nozzle throat
therm	thermal
y	ejector choking section
1, 2, 3, f	cross-sections of the ejector (Fig. 3, Eqs. (2)–(4))
1, 2, 3…9	cycle states in the Figs. 1–2, Eq. (6)

1. Introduction

The widespread use of cooling and air-conditioning systems in summer causes a serious electrical peak load problem, and electrical power generation has an environmental impact as well. There are many thermal energy types in the world, including solar thermal, waste and exhaust heat, and geothermal and biomass energy. For several decades, scientists have been looking for a suitable cooling technology that can be powered directly by thermal energy. A heat-driven ejector cooling cycle looks very promising for this need and offers interesting alternatives for air conditioning and space cooling.

The New Energy Center at National Taiwan University has long been devoted to the development of solar ejector cooling technology, particularly with ejector refrigeration machines (ERMs) operating with low-boiling point working fluids (Huang et al., 1985, 1999, 2010a, 2010b). These machines have several advantages over other heat-driven refrigeration cycles, including low temperature heat supply, simplicity in design and operation, the possibility of freezing-temperature operation, high reliability, and low installation cost. These make ERMs more attractive than other heat-driven refrigeration cycles and represent a real opportunity for the further development and wide application of these cooling machines. At present, the relatively low coefficients of performance (COPs) of ERMs are the main reason that they are rarely used. This low efficiency is caused mainly by irreversibilities in the ejector. In order to increase the COP values, it is necessary first of all to improve the performance of the ejector.

Many researchers have recently studied, both theoretically and experimentally, low-boiling refrigerants in ERMs (Sun, 1999; Cizungu et al., 2001; Selvaraju and Mani, 2004, 2006). A comparison of system performance was carried out for the same ejector geometry using the environmentally friendly working fluids R123, R134a, R152a, and R717. The results suggested that, for different boiler temperatures, the entrainment ratio and the system efficiency depend mainly on the ejector geometry and the compression ratio.

The basic ejector theory was developed by Munday and Bagster in 1977. Many other research studies have been carried out to investigate the performance of the ejector refrigeration cycle with different refrigerants. The structure of the ejector has a great influence on the performance of the ejector. Recently, computational fluid dynamics (CFD) analysis has provided a powerful tool for the study of supersonic ejectors (Sriveerakul et al., 2007a, 2007b; Scott et al., 2008; Varga et al., 2009).

An improved 1-D model for the prediction of the entrainment ratio ω, and an optimal design for ejectors with cylindrical and conical-cylindrical mixing chambers are presented in this paper. The governing equations were derived on the basis of one dimensional model of Sokolov and Zinger (1989).

2. Theoretical analysis of ejector design and ejector refrigeration cycle performance

The main components of an ERM include an ejector, a generator, an evaporator, a condenser, an expansion valve, and a feed pump. Fig. 1 shows the arrangement of these components. The process of a continuously operating ERM is characterized by points 1–9 in Fig. 2, which is a thermodynamic ejector refrigeration cycle in the pressure-enthalpy diagram. A low-boiling refrigerant is heated and vaporized in

the generator using thermal energy Q_g at relatively high pressure P_g. This primary vapor, with a mass flow rate of $\dot{m}_p$, passes through the supersonic nozzle, drawing secondary vapor with a mass flow rate of $\dot{m}_s$ into the ejector from the evaporator. The two streams mix in the ejector and leave it after the recovery of pressure in the ejector's diffuser. The combined stream flows to the condenser, where it is condensed to liquid at intermediate pressure P_c. The heat of condensation Q_c is released into the environment.

From the condenser, a portion of the liquid is returned to the generator via an electrically driven feed pump, consuming mechanical work $\dot{W}_{mech}$, while the remainder is expanded through an expansion valve. Thereafter, the vapor–liquid flow of the refrigerant enters the evaporator, where the liquid is evaporated at low temperature T_e and pressure P_e to produce the necessary cooling effect Q_e. The vapor from the evaporator is finally entrained by the ejector, thus completing the cycle.

From the aforesaid, it follows that the supersonic ejector is the key component in the ejector cooling cycle, and supplies suction, compression, and discharge of the secondary vapor by using the primary vapor. Two choking phenomena exist in ejector performance: one in the primary flow through the supersonic nozzle and the other in the suction flow in the mixing chamber (Huang et al., 1985).

Fig. 3 illustrates the structure of supersonic ejectors with (a) cylindrical and (b) conical-cylindrical mixing chambers.

The geometry of the ejector is characterized by the configuration of the nozzle (A_t – the primary nozzle throat area; A_1 – the primary nozzle exit area) and the cross-section areas of the other parts of the ejector (A_2 – the entrance area of the mixing chamber; A_3 – the area of the cylindrical section of the mixing chamber).

The operating conditions of an ejector are specified by operating pressures P_e, P_c, and P_g, the expansion pressure ratio, $E = P_g/P_e$, and the compression pressure ratio, $C = P_c/P_e$.

The performance of an ejector is measured by its entrainment ratio ω, which is defined as:

$$\omega = \frac{\dot{m}_s}{\dot{m}_p} \tag{1}$$

The design of an ejector flow profile with a CMC is defined by the area ratio α, which can be found from the relation:

$$\alpha = \frac{A_3}{A_t} \tag{2}$$

The primary nozzle design is determined by the area ratio:

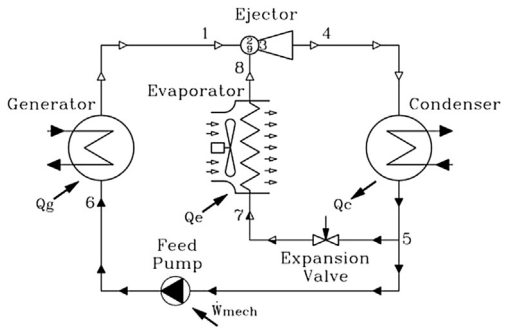

Fig. 1 – Diagram of an ejector refrigeration machine.

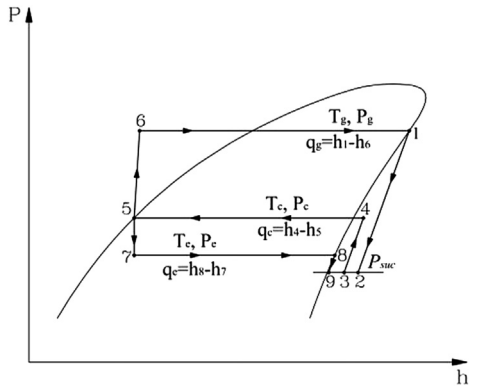

Fig. 2 – Diagram of the ejector refrigeration cycle.

$$\phi = \frac{A_1}{A_t} \tag{3}$$

The most important geometrical parameters of the ejector are the area ratios A_3/A_t and A_1/A_t. When the value of A_3/A_t is low, the jet devices have a high compression pressure ratio C, but the entrainment ratio ω is low. When the value of A_3/A_t increases, the compression pressure ratio C decreases, but the entrainment ratio ω increases. The second geometrical parameter A_1/A_t determines the pressure of the working vapor at the exit of the nozzle. Insufficient or excessive expansion of the working fluid in the nozzle results in an increase in energy loss during the outflow and in a decrease in ejector efficiency.

The design of a CCMC is specified by the area ratio α, the converging angle ψ at the mixing chamber entrance, and the area ratio β, which is given as:

$$\beta = \frac{A_2}{A_3} \tag{4}$$

Construction, geometry, and the surface condition of the supersonic ejector flow profile must provide the most effective utilization of primary flow energy for suction, compression,

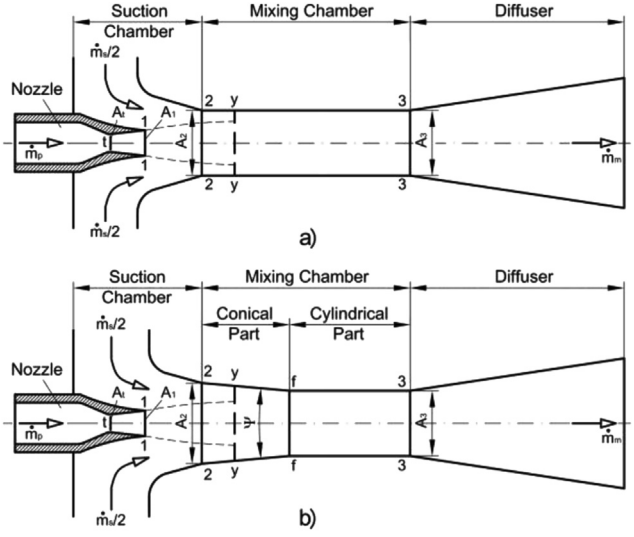

Fig. 3 – Structure of ejectors with (a) cylindrical and (b) conical-cylindrical mixing chambers.

and discharge of the secondary vapor (Petrenko, 1978; Huang et al., 1999; Petrenko et al., 2005a, 2005b; Eames et al., 2007).

To maintain optimum performance, the geometry of the ejector flow profile must be varied. This variation in geometry should first take place in the primary nozzle throat area A_t and in mixing chamber area A_3.

On the basis on the improved 1-D theory of ejector design, the area ratio α and the optimum value of β can be found by making use of variational calculation. The value of β_{opt} corresponds to the maximum entrainment ratio ω. Supplementary data for the determination of the α, β_{opt}, and the optimal converging angle ψ are given in Petrenko (1978) and Petrenko et al. (2005a).

Two kinds of energies are required to drive the ejector cooling cycle: thermal energy Q_g input to the generator, and mechanical (electrical) energy $\dot{W}_{mech}$ to power the feed pump. Since these energies are obtained from two dissimilar sources, with entirely different specific energy values and prices, the performance of the ERM can be correctly specified by equal use of two COPs, namely COP_{therm} and COP_{mech} (Petrenko, 2001, 2009). The value of COP_{therm} is defined as Q_e divided by Q_g, and the value of COP_{mech} is the ratio between Q_e and the mechanical power $\dot{W}_{mech}$ used by the mechanical feed pump. They can be expressed as Eqs. (5) and (6):

$$COP_{therm} = \frac{Q_e}{Q_g} = \frac{\dot{m}_s q_e}{\dot{m}_p q_g} = \omega \frac{q_e}{q_g}, \tag{5}$$

$$COP_{mech} = \frac{Q_e}{\dot{W}_{mech}} = \frac{\eta_{fp}\dot{m}_s q_e}{\dot{m}_p v_5 (P_g - P_c)} = \frac{\eta_{fp}\omega q_e}{v_5 (P_g - P_c)}, \tag{6}$$

where v_5 and η_{fp} are the specific volume of refrigerant intake and the feed pump coefficient of efficiency, respectively; $(P_g - P_c)$ is the generating and condensing pressure difference, in kPa.

According to Eq. (5), in order to increase COP_{therm}, it is necessary to raise the entrainment ratio ω and the specific cooling capacity q_e, as well as decrease the specific generating heat q_g. At the specified evaporating temperature T_e this requires the generating temperature T_g to be increased and the condensing temperature T_c to be decreased. From Eq. (6), it follows that in order to increase COP_{mech}, it is necessary to raise the entrainment ratio ω, the specific cooling capacity q_e and the feed pump coefficient of efficiency η_{fp}, and to decrease the pump pressure difference $(P_g - P_c)$. Thus, analysis of Eqs. (5) and (6) shows that the characteristics of COP_{therm} and COP_{mech} depend strongly on the operating conditions, the efficiency of the ejector used, and the thermodynamic properties of the refrigerant used. Maximum efficiency can only be obtained if the cycle of the ERM is completely reversible.

Obviously, reliable performance of ERMs greatly depends on the reliability of feed pump operation, which is the critical component in the ejector cycle. This electrically actuated pump is the only element in the heat-driven ERM that has moving parts, and it therefore determines the operational safety, leak resistance, and lifetime of the whole system.

The safe performance and coefficient of efficiency of the feed pump are largely dependent on the pressure difference $(P_g - P_c)$. To decrease this pressure difference, and thus to increase the dependability and effectiveness of the system as a whole, the use of low-pressure refrigerants in the ejector cycle is preferable.

3. Ejector analysis and performance

The design equations for the 1-D mathematical model for the prediction of the entrainment ratio ω, and the optimal design for ejectors with a CMC and conical-cylindrical mixing chambers (CCMC) presented in this paper were derived on the basis of the one-dimensional model of Sokolov and Zinger (1989).

A schematic view of an ejector with cylindrical and conical-cylindrical mixing chambers is shown in Fig. 3.

The following assumptions were made for the analysis:

1. primary and secondary flows have identical adiabatic indexes γ and the universal gas constant R;
2. before entering the mixing chamber in the section between the output cross-section of the nozzle (exit of the nozzle) 1–1 and the inlet cross-section of the mixing chamber 2–2, the primary flow does not expand and does not mix with the entrained flow;
3. the thickness of the output cross-section of the nozzle edge is negligible;
4. in cross-section y–y both flows have static pressure that is equal to the critical pressure of the entrained flow, i.e., $P_{py} = P_{sy} = P_s \cdot \Pi_{sx}$;
5. initial velocities of the primary and secondary flows are negligible because they are much lower compared to the velocities of these flows in the mixing chamber.

Three laws define the processes that refer to all jet devices:

– the mass-conservation law:

$$\dot{m}_m = \dot{m}_p + \dot{m}_s = \dot{m}_p(1 + \omega), \tag{7}$$

– the energy-conservation law:

$$h_p \cdot \dot{m}_p + h_s \cdot \dot{m}_s = h_m \cdot \dot{m}_m \tag{8}$$

– the momentum-conservation law:

$$\varphi_2 \cdot (\dot{m}_p \cdot V_{p2} + \dot{m}_s \cdot V_{s2}) - (\dot{m}_p + \dot{m}_s) \cdot V_3 = P_3 \cdot A_3 + \int_{A_2}^{A_3} P \, dA - P_{p2} \cdot A_{p2} - P_{s2} \cdot A_{s2}. \tag{9}$$

The value of $\int_{A_2}^{A_3} P \, dA$ represents the momentum caused by the reaction of the wall of the conical entrance region under the constant-pressure condition; this value can be calculated from Eq. (10):

$$\int_{A_2}^{A_3} P \, dA = 0.5 \cdot A_3 \cdot (\beta - 1) \cdot (P_{s2} + P_3 \cdot \Pi_{3f}), \tag{10}$$

where Π_{3f} is a pressure ratio at the entrance and exit of the cylindrical part of the mixing chamber, it can be found from:

$$\Pi_{3f} = \frac{P_f}{P_3} = \left(\frac{P_2}{P_3}\right)^{\delta} = \left(\frac{P_s}{P_m}\right)^{\delta} \cdot \left(\frac{\Pi_{s2}}{\Pi_{m3}}\right)^{\delta},$$

$$\delta = \frac{\lg \frac{P_3}{P_f}}{\lg \frac{P_3}{P_2}} = \frac{\lg P_3 - \lg P_f}{\lg P_3 - \lg P_2}.$$

3.1. Gas dynamic functions

Gas dynamic functions are used for the prediction of the entrainment ratio ω in methodology of Sokolov and Zinger (1989), which make calculation of ejector entrainment ratio easier.

- The reduced isentropic velocity λ is defined as a ratio of flow velocity V_a during its isentropic (adiabatic) flow and critical velocity V_x:

$$\lambda = \frac{V_a}{V_x}, \tag{11}$$

where V_x can be calculated as:

$$V_x = \sqrt{\frac{2\cdot\gamma}{\gamma+1}\cdot\frac{P_0}{\rho_0}}, \tag{12}$$

P_0 and ρ_0 are the pressure and the specific density respectively at stagnation condition.

The reduced pressure Π is defined as a ratio of the pressure P of the isentropic moving gas in a given cross-section and a stagnation pressure P_0:

$$\Pi = \left[1-\frac{\gamma-1}{\gamma+1}\cdot\lambda^2\right]^{\frac{\gamma}{\gamma-1}} \tag{13}$$

The reduced mass velocity ε is defined as a ratio of the area of flow critical cross-section A_x and the area of flow cross-section A (Sokolov and Zinger (1989)):

$$\varepsilon = \frac{A_x}{A} = \lambda_{max}\cdot\left(\frac{\Pi}{\Pi_x}\right)^{\frac{1}{\gamma}}\cdot\sqrt{1-\Pi^{\frac{\gamma-1}{\gamma}}} = \left(\frac{\gamma+1}{\gamma}\right)^{\frac{\gamma}{\gamma-1}}\cdot\lambda\cdot\left(1-\frac{\gamma-1}{\gamma+1}\cdot\lambda^2\right)^{\frac{1}{\gamma-1}}, \tag{14}$$

where

$$\lambda_{max} = \sqrt{\frac{\gamma+1}{\gamma-1}}, \tag{15}$$

$$\Pi_x = \left(\frac{2}{\gamma+1}\right)^{\frac{\gamma}{\gamma-1}}. \tag{16}$$

3.2. Governing equations

The velocities of primary, secondary, and mixed flows V_{p2}, V_{s2}, and V_3 in typical cross-sections of the mixing chamber can be expressed as follows:

$$V_{p2} = \varphi_1\cdot a_{px}\cdot\lambda_{p2},\quad a_{px} = \sqrt{\frac{2\cdot\gamma}{\gamma+1}\cdot\frac{P_p}{\rho_p}}, \tag{17}$$

$$V_{s2} = \varphi_4\cdot a_{sx}\cdot\lambda_{s2},\quad a_{sx} = \sqrt{\frac{2\cdot\gamma}{\gamma+1}\cdot\frac{P_s}{\rho_s}}, \tag{18}$$

$$V_3 = \frac{a_{mx}}{\varphi_3}\cdot\lambda_{m3},\quad a_{mx} = \sqrt{\frac{2\cdot\gamma}{\gamma+1}\cdot\frac{P_m}{\rho_m}}. \tag{19}$$

The areas of primary, secondary and mixed flows can be determined from Eqs. (20)–(22):

$$A_{p2} = \frac{\dot{m}_p\cdot a_{px}}{\gamma_p\cdot\Pi_{px}\cdot P_p\cdot\varepsilon_{p2}}, \tag{20}$$

$$A_{s2} = \frac{\dot{m}_s\cdot a_{sx}}{\gamma_s\cdot\Pi_{sx}\cdot P_s\cdot\varepsilon_{s2}}, \tag{21}$$

$$A_3 = \frac{(\dot{m}_p+\dot{m}_s)\cdot a_{mx}}{\gamma_m\cdot\Pi_{mx}\cdot P_m\cdot\varepsilon_{m3}}. \tag{22}$$

The velocities of flows in typical cross-sections are expressed through critical velocities of working flow (a_{px}), entrained flow (a_{sx}), and mixed flow (a_{mx}), as follows from Eqs. (17)–(19). If the critical velocities if the flows are known, the critical cross-sections of the working, entrained, and mixed flows can be determined from Eqs. (20)–(22). From these equations the ejector flow profile can be built. These equations result from the mass conservation law (Eq. (7)).

After substitution of expressions (17–19) for velocities V_{p2}, V_{s2}, and V_3, expressions (20–22) for cross-sections of flows A_{p2}, A_{s2}, and A_3, the values of static pressures $P_{s2} = \Pi_{s2}\cdot P_s$ and $P_3 = P_m\cdot\Pi_{m3}$, and the value of momentum from the reaction of the entry converge for the cone wall, that is Eq. (10) into Eq. (9) according to the mass-conservation law (7), we get Eq. (23) for the calculation of the entrainment ratio of the ejector working with the substances with the same physical properties (Sokolov and Zinger (1989)):

$$\omega = \frac{K_1\cdot\lambda_{p2}-\lambda_{m3}-K_3}{\lambda_{m3}+K_4-K_2\cdot\lambda_{s2}}\cdot\frac{1}{\sqrt{\Theta}}, \tag{23}$$

Here,

$$K_1 = \varphi_1\cdot\varphi_2\cdot\varphi_3, \tag{24}$$

$$K_2 = \varphi_2\cdot\varphi_3\cdot\varphi_4, \tag{25}$$

$$K_3 = \frac{\varphi}{\varepsilon_{p2}}\cdot\frac{P_m}{P_p}\cdot\left\{\Pi_{m3}-\frac{P_s}{P_m}\cdot\left(\beta-0.5\cdot(\beta-1)\cdot\Pi_{s2}\times\left[1+\left(\frac{P_m}{P_s}\right)^{1-\delta}\cdot\left(\frac{\Pi_{m3}}{\Pi_{s2}}\right)^{1-\delta}\right]\right)\right\}, \tag{26}$$

$$K_4 = \frac{\varphi}{\varepsilon_{s2}}\cdot\frac{P_m}{P_s}\cdot\left\{\Pi_{m3}-\Pi_{m2}\cdot\left(\beta-0.5\cdot(\beta-1)\times\left[1+\left(\frac{P_m}{P_s}\right)^{1-\delta}\cdot\left(\frac{\Pi_{m3}}{\Pi_{s2}}\right)^{1-\delta}\right]\right)\right\}, \tag{27}$$

$$\varphi = \frac{\varphi_3}{\gamma\cdot\Pi_x\cdot\beta}, \tag{28}$$

$$\Theta = \frac{T_s}{T_p} = \frac{a_{sx}^2}{a_{px}^2} \tag{29}$$

φ_1, φ_2, φ_3 and φ_4 are the experimental velocity coefficients of the nozzle, mixing chamber, diffuser, and entrance part of the mixing chamber, respectively (those allow for accounting the irreversibility of the flow through ejector);

δ is the coefficient characterizing the increment of pressure at the conical part of the mixing chamber;

Θ is the dimensionless temperature.

It can be seen from these equations that it is necessary for the determination of ω to have gas-dynamic functions of the primary and secondary flows in the inlet cross-section of

mixing chamber (λ_{p2}, Π_{p2}, ε_{p2} and λ_{s2}, Π_{s2}, ε_{s2}) and of the mixed flow at the exit from the mixing chamber (λ_{m3}, Π_{m3}, ε_{m3}).

Gas-dynamic functions of the primary flow are determined from Eq. (30):

$$\lambda_{p2} = \lambda_{max} \cdot \sqrt{1 - \left(\frac{P_s}{P_p}\right)^{\frac{\gamma-1}{\gamma}}}, \quad \varepsilon_{p2} = \lambda_{p2} \cdot \left(\frac{P_s}{P_p} \cdot \frac{1}{\Pi_x}\right)^{\frac{1}{\gamma}}. \tag{30}$$

The properties of the entrained flow in the cross-section 2–2, and of the mixed flow in cross-section 3–3 cannot be selected optionally, since they are related through the geometry of the mixing chamber.

Reciprocally, they are connected by Eq. (31) (Sokolov and Zinger (1989):

$$\varepsilon_{s2} = \frac{\omega \cdot \sqrt{\Theta}}{\beta \cdot (1 + \omega \cdot \sqrt{\Theta}) \cdot \frac{P_s}{P_m} \cdot \frac{1}{\varepsilon_{m3}} - \frac{P_s}{P_p} \cdot \frac{1}{\varepsilon_{p2}}}. \tag{31}$$

The goal of the calculation consists in determining the optimum gas-dynamic functions λ_{s2} and λ_{m3} of these flows, namely, the value at which the entrainment ratio ω peaks.

To properly solve this problem, it is necessary to impose certain limitations on the ejector operating at choking condition.

3.3. Limitations on the ejector operating at choking condition

The basis of the one-dimensional model of Sokolov and Zinger is the theory of the limiting regimes occurring at choking condition (Sokolov and Zinger, 1989).

In one-dimensional analysis, there are three possible locations where limiting regime can occur: (I) at the inlet cross-section 2–2 of the mixing chamber; (II) somewhere along the entrance section y–y of the mixing chamber; and (III) at the exit cross-section 3–3 of the mixing chamber before the inlet to the diffuser (Sokolov and Zinger, 1989; Guangming et al., 2010).

Considering the above, limiting regime I occurs when the secondary flow reaches sonic velocity at cross section 2–2, and therefore, the value λ_{s2} must not exceed 1.

When the ejector operates at limiting regime III, the velocity of the mixed flow at the exit section of the mixing chamber 3–3 cannot be higher than the critical velocity, and the value of λ_{m3} must not exceed 1.

When the ejector operates at limiting regime II, the velocity of the secondary flow at cross-section y–y cannot be higher than the critical value; therefore, the value of λ_{sy} must not exceed 1.

By analogy with Eq. (31), the reduced mass velocity of the secondary flow ε_{sy} at the section y–y is determined from:

$$\varepsilon_{sy} = \frac{\omega}{\sigma \cdot (1 + \omega) \cdot \frac{a_{mx}}{a_{sx}} \cdot \frac{P_s}{P_m} \cdot \frac{1}{\varepsilon_{m3}} - \frac{a_{mx}}{a_{sx}} \cdot \frac{P_s}{P_p} \cdot \frac{1}{\varepsilon_{p2}}}, \tag{32}$$

where $\sigma = A_y/A_3$, $\sigma = 1$ for an ejector with a cylindrical mixing chamber, and $1 < \sigma < \beta$ for an ejector with a conical-cylindrical mixing chamber.

Since the velocity of the secondary flow V_{sy} at cross-section y–y equals the critical velocity V_{sx} at limiting regime II, the value $\varepsilon_{sy} = \varepsilon_{sx} = 1$.

On the basis of Eq. (32), the value of ω, which corresponds to limiting regime II, can be calculated by:

$$\omega = \frac{\sigma \cdot \frac{P_s}{P_m} \cdot \frac{1}{\varepsilon_{m3}} - \frac{P_s}{P_m} \cdot \frac{1}{\varepsilon_{py}}}{1 - \sigma \cdot \frac{P_s}{P_m} \cdot \frac{1}{\varepsilon_{m3}}} \cdot \frac{1}{\sqrt{\Theta}}. \tag{33}$$

3.4. Optimization of gas-dynamic functions determination

According to the methodology of Sokolov and Zinger (1989), the optimum gas-dynamic functions λ_{s2} and λ_{m3} determining by the linear method of successive approximation, which is laborious and has low calculation accuracy.

As an alternative to the Sokolov and Zinger method, the authors offer a new approach for the determination of the maximum entrainment ratio. This method consists in solving of a nonlinear programming problem for objective function, which has the form:

$$\omega = \omega(x_1,\ x_2,\ z_1,\ z_2 \ldots z_i) \Rightarrow MAX, \tag{34}$$

under the following constraints:

$$ceq_i(x_1,\ x_2,\ z_1,\ z_2 \ldots z_k) = 0, \quad i = 1,\ 2 \tag{35}$$

$$0 < x_n \leq 1, \quad n = 1,\ 2,\ 3, \tag{36}$$

where x_1, x_2 are the independent variables; and z_1, z_2,..., z_k denote the parameters of the objective function.

For specific physical quantities, problem (34–36) is represented by the following. The objective function is presented by the expression:

$$\omega = \frac{K_1 \cdot \lambda_{p2} - \lambda_{m3} - K_3}{\lambda_{m3} + K_4 - K_2 \cdot \lambda_{s2}} \cdot \frac{1}{\sqrt{\Theta}} \tag{37}$$

for determination of the entrainment ratio (23), where $\lambda_{s2} = x_1$ and $\lambda_{m3} = x_2$ are independent variables; x_1 is the reduced isentropic velocity of the secondary flow at the entrance section of the mixing chamber λ_{s2}; x_2 is the reduced isentropic velocity of the mixed flow at the exit section of the mixing chamber λ_{m3}.

Nonlinear restrictions $ceq_i(x_1,\ x_2,\ z_1,\ z_2 \ldots z_k) = 0$ can be written as the following equations:

$$\begin{aligned} ceq_1 = &\left(\sigma - \frac{P_m}{P_p} \cdot \frac{\varepsilon_{m3}}{\varepsilon_{py}}\right) \cdot (\lambda_{m3} + K_4 - K_2 \cdot \lambda_{s2}) \\ &- \left(\sigma - \frac{P_m}{P_s} \cdot \varepsilon_{m3}\right) \cdot (\lambda_{m3} + K_3 - K_1 \cdot \lambda_{p2}) = 0, \end{aligned} \tag{38}$$

$$\begin{aligned} ceq_2 = &\left(\sigma - \frac{P_m}{P_p} \cdot \frac{\varepsilon_{m3}}{\varepsilon_{py}}\right) \cdot \left(\beta - \frac{P_m}{P_s} \cdot \frac{\varepsilon_{m3}}{\varepsilon_{s2}}\right) \\ &- \left(\sigma - \frac{P_m}{P_s} \cdot \varepsilon_{m3}\right) \cdot \left(\beta - \frac{P_m}{P_p} \cdot \frac{\varepsilon_{m3}}{\varepsilon_{p2}}\right) = 0. \end{aligned} \tag{39}$$

Linear restrictions on the nonlinear programming problem, in the form of $0 < x_n \leq 1$, can be written as the following equations:

$$0 < \lambda_{m3} \leq 1, \quad 0 < \lambda_{s2} \leq 1, \quad 0 < \lambda_{sy} \leq 1, \tag{40}$$

It is worth noting that the linear restriction $0 < \lambda_{sy} \leq 1$ for the objective function (38) is implicit, and it reveals a nonlinear restriction (39).

The problem of nonlinear programming (37–39) is solved by gradient methods in the environment of the computer mathematics package MatLab by means of the add-on module Optimization Toolbox. The advantages of the suggested method with the use of modern computer technologies are in totally automating the determination of the entrainment ratio maximum for different refrigerants in a wide range of operating conditions, as well as in its high accuracy and calculating speed. The values of the gas-dynamic functions, λ_{m3} and λ_{s2}, obtained from solving the problems (37–39), were substituted into Eqs. (23), (26) and (27), from which the maximum of entrainment ratio ω was determined.

Automating the calculation of the entrainment ratio maximum makes it possible to determine the optimal value of β for an ejector with a CCMC. The simulation flowchart for the optimal value of β determination when the maximum of the entrainment ratio for the given design conditions is reached, is shown in Fig. 4.

Analysis of Eqs. (26–27), (32–33), and (38–39) shows that to determine the entrainment ratio of an ejector with a CCMC, in addition we must have the values of φ_1, φ_2, φ_3, φ_4, β, σ, and δ. Hereinafter the following experimental constants were used: $\varphi_1 = 0.95$, $\varphi_2 = 0.975$, $\varphi_3 = 0.9$, $\varphi_4 = 0.925$, $\delta = 0.5$, and $\sigma = \beta$ (Sokolov and Zinger, 1989; Guangming et al., 2010).

4. Determination of the ejector geometry

The operating conditions for which the ejector and ERM were developed for the selected refrigerants were characterized by the design parameters of the ejector cooling cycle T_e, P_e, T_c, P_c, T_g, and P_g, and by the cooling capacity of Q_e. The values of T_e and Q_e were assigned in accordance with the requirements of refrigeration users. The temperature T_c was selected on the basis of the design parameters of the ambient environment and the mode of rejection of condensation heat. The value of T_g was determined by taking into account the temperature and the kind of heating medium, the mode of generation of the heat supply, and the properties of the refrigerant used.

To determine the geometry of the ejector and the design values of ERM, it is necessary to build its cycle and to determine the specific heat load q_e. On the basis of the methodology developed in Section 3 of this paper, the design value of the entrainment ratio maximum ω_{max} was calculated. Mass flow rate of entrained flow $\dot{m}_s$ was determined from the given cooling capacity:

$$\dot{m}_s = \frac{Q_e}{q_e} = \frac{Q_e}{h_8 - h_7}, \tag{41}$$

Mass flow rate of primary flow $\dot{m}_p$ was determined from Eq. (1):

$$\dot{m}_p = \frac{\dot{m}_s}{\omega_{max}}. \tag{42}$$

The computed values of $\dot{m}_s$ and $\dot{m}_p$ were then used to design the ejector and to determine the calculated geometries, which were intended to provide maximum efficiency of operation at the rated conditions.

For the determination of cross-section areas A_t, A_1, and A_2 of the ejector flow profile (Fig. 3), the following equations were used (Sokolov and Zinger (1989):

$$A_t = \frac{\dot{m}_p \cdot a_{px}}{\gamma \cdot \Pi_x \cdot P_p}, \tag{43}$$

$$A_1 = \frac{A_t}{\varepsilon_{p2}}, \tag{44}$$

$$A_2 = A_1 + A_{s2}, \tag{45}$$

where

$$A_{s2} = \frac{\dot{m}_s \cdot a_{sx} \cdot \varepsilon_{s2}}{\gamma \cdot \Pi_x \cdot P_s}. \tag{46}$$

For the ejector with a CMC, the area of the exit cross-section was $A_3^I = A_2$, while the value of A_3^{II} for the ejector with a CCMC was determined from the following equation:

$$A_3^{II} = \frac{A_2}{\beta_{opt}} \tag{47}$$

The main geometric parameter of the ejector A_3/A_t, which provides the design value ω, was calculated from Eq. (48):

$$\frac{A_3}{A_t} = \frac{P_p\left(1 + \omega\sqrt{\theta}\right)}{P_m \varepsilon_{m3}}. \tag{48}$$

The area ratio of the nozzle A_1/A_t was found from:

$$\frac{A_1}{A_t} = \frac{1}{\varepsilon_{P1}}. \tag{49}$$

5. Refrigerant selection for the experimental ERM

The analysis and comparison of performance characteristics for various refrigerants showed that, from thermodynamic

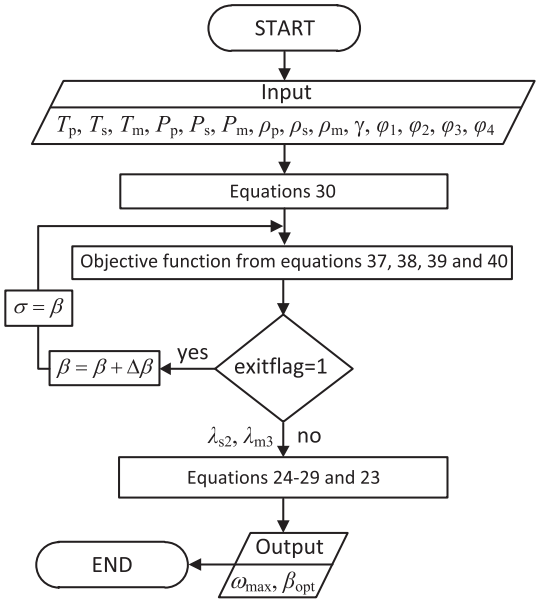

Fig. 4 – Simulation flowchart for the determination of the optimal value of β and the maximum value of ω.

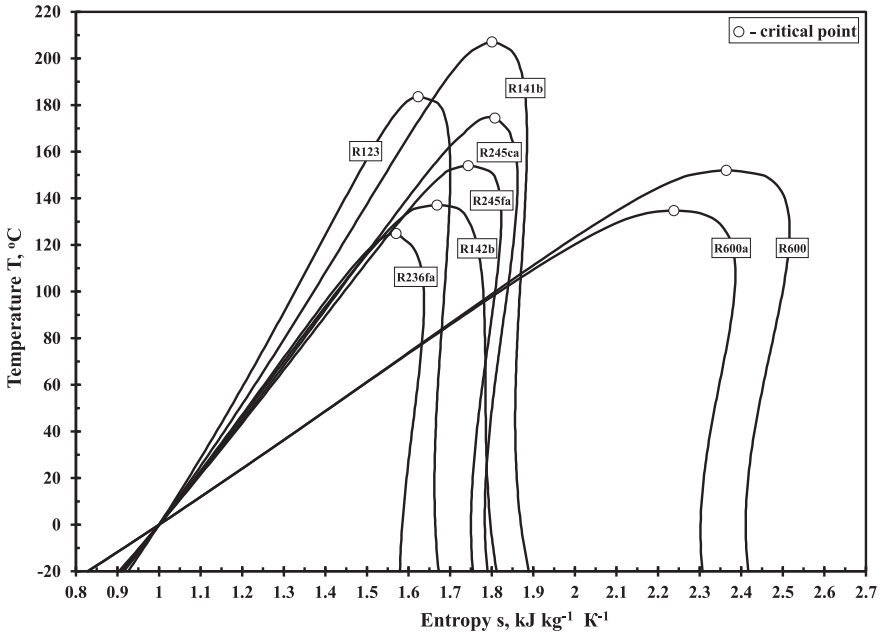

Fig. 5 – Saturation curves of different low-pressure refrigerants in a T-s diagram.

and operating viewpoints, the most suitable refrigerants for ERMs were low-pressure types with a high critical temperature T_{cr}, a large specific latent heat of vaporization at temperatures T_e and T_g, a low specific heat of the liquid refrigerant in the range of operating temperatures (T_g–T_e), and a normal boiling point temperature T_b about T_e (Petrenko, 2001; Petrenko et al., 2005a; Mazur, 2003).

Fig. 5 shows saturation curves of eight low-pressure working fluids, including two hydrocarbons, in a *T-s* diagram, and Table 1 presents several parameters of these refrigerants for comparison, in order to allow selection of the most appropriate one.

Hydrocarbons are well-known gases and can be found in a number of general applications. Their use in systems for commercial refrigeration, chillers, and heat pumps is well established (Granryd, 2001). Results of investigations of ERMs operating with various hydrocarbon refrigerants have also been reported in recent years (Selvaraju and Mani, 2004; Pridasawas and Lundqvist, 2007; Nehdi et al., 2008; Boumaraf and Lallemand, 2009; Roman and Hernandez, 2009, 2011). Several hydrocarbons have favorable characteristics as refrigerants from a thermodynamic as well as a heat transfer point of view. They have excellent environmental characteristics: no ozone depleting potential and negligible global warming potential. Hydrocarbons have been used as refrigerants for many years in the petrochemical industry. Experience gained in recent years indicates that hydrocarbons can be implemented in an economical way for a number of other applications. However, safety precautions due to their flammability must be seriously taken into account (Granryd, 2001).

From Fig. 5 and Table 1 it follows that all the low-pressure refrigerants presented have not only relatively high critical temperatures and rather low critical and operating pressures, but also positive-slope saturated-vapor lines, except refrigerant R142b, which has an almost vertical saturated-vapor line.

Table 1 – Characteristics of different low-pressure refrigerants.

Property	Refrigerant							
	R123	R141b	R142b	R236fa	R245ca	R245fa	R600	R600a
Chemical Formula	$C_2F_3HCl_2$	$C_2FH_3Cl_2$	$C_2H_3F_2Cl$	$C_3H_2F_6$	$C_3H_3F_5$	$CHF_2CH_2CF_3$	C_4H_{10}	C_4H_{10}
Molecular Weight M, kg kmol^{-1}	152.93	116.9	100.5	152.04	134.05	134.05	58.13	58.13
Normal Boiling Temperature T^b, °C	27.87	32.20	−9.80	−1.44	25.13	14.90	−0.50	−11.61
Critical Temperature T^{cr}, °C	183.8	208.0	137.4	124.92	174.4	154.05	152.0	134.7
Critical Pressure P^{cr}, bar	36.7	43.4	42.0	32.0	39.3	36.4	37.9	36.4
Specific Heat Capacity of Liquid c^p at $T = 30$ °C, kJ kg^{-1}K^{-1}	1.025	1.15	1.19	1.28	1.34	1.37	2.47	2.49
Latent Heat r at $T = 8$ °C, kJ kg^{-1}	178.3	234.0	209.4	155.4	210.0	200.6	377.9	347.8
Ozone Depletion Potential	0.02	0.11	0.06	0.00	0.00	0.00	0.00	0.00
Global Warming Potential	76	630	2270	6300	950	950	<10	<10
Flammability	No	Yes	Yes	No	No	No	Yes	Yes

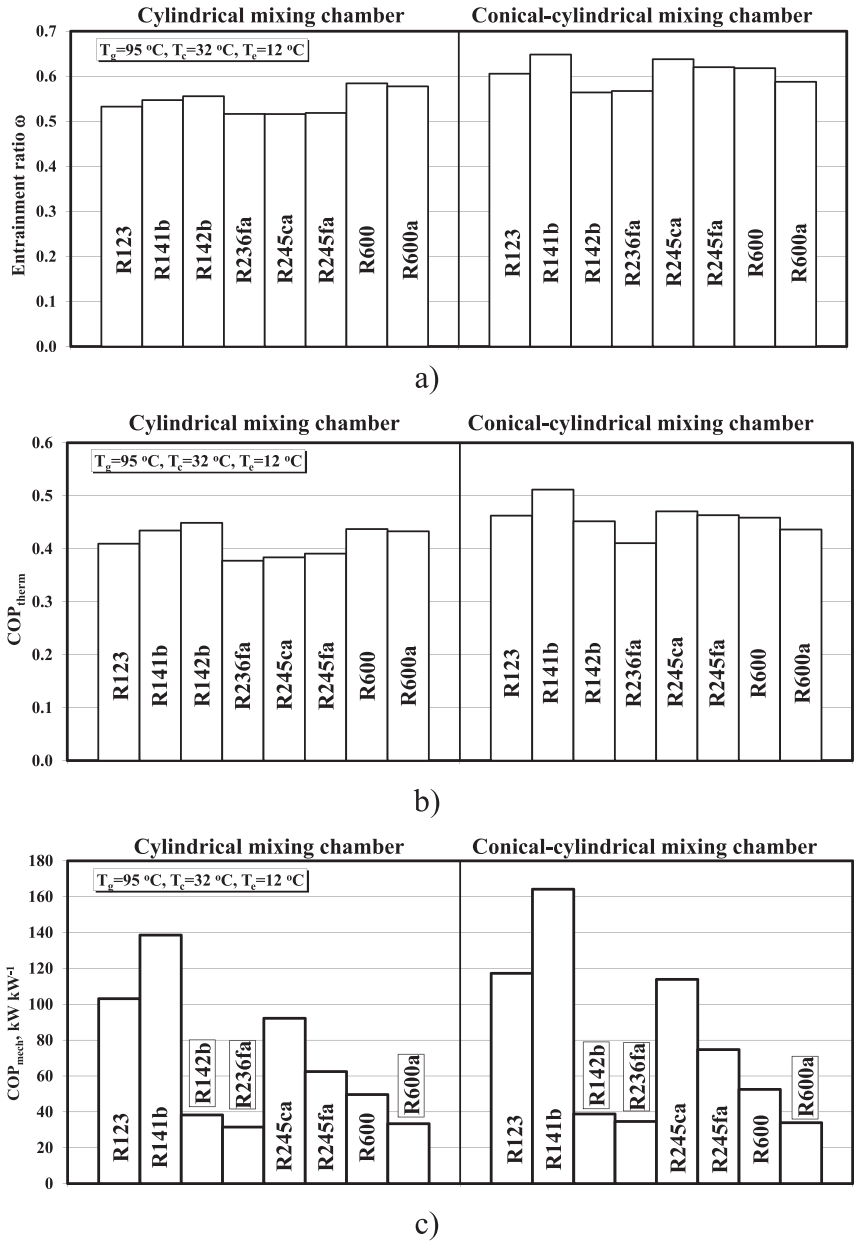

Fig. 6 – Comparison of the entrainment ratio ω (a), COP_{therm} (b), and COP_{mech} (c) for different refrigerants.

Therefore, the actual near-isentropic expansion of the saturated vapor of all these working fluids in the nozzle of the ejector is realized in the dry-vapor regions with beneficial effects on the reliability of the flow-through parts of the ejector, as well as on the performance of the ejector.

The analysis and comparison of performance characteristics ω, COP_{therm}, and COP_{mech} of these refrigerants for design conditions of $T_g = 95°C$, $T_c = 32°C$, and $T_e = 12°C$ and of $\eta_{fp} = 0.5$ for ejectors with a CMC or a CCMC are shown in Fig. 6.

From Fig. 6a, we observe that, for different refrigerants, the values of ω vary across a range of 0.52–0.58 for the CMC and from 0.56 to 0.65 for the CCMC. Fig. 6b shows the variation in COP_{therm} whose small range of change is similar to the variation of the entrainment ratio ω. The range of COP_{therm} is from 0.38 to 0.45 for the CMC and from 0.41 to 0.51 for the CCMC. This proves the importance of improving ejector design in order to obtain the maximum entrainment ratio, which in turn will maximize cycle performance.

Fig. 6c indicates clearly, in contrast to Fig. 6a and b, that the discrepancy of COP_{mech} is much bigger than ω and COP_{therm}: from 33.36 to 138.56 kW kW^{-1} for the CMC and from 33.93 to 164.18 kW kW^{-1} for the CCMC. This contrast is caused by the contribution of the pressure difference ($P_g - P_c$) and the specific cooling capacity q_e of various refrigerants. It follows from this that refrigerants with a smaller pressure difference ($P_g - P_c$) and a larger latent heat can make full use of the COP_{mech}. On the other hand, the refrigerants with a higher ω and COP_{therm} and a lower pressure difference ($P_g - P_c$), such as

R141b, R123, and R245ca, have a normal boiling point temperature T_b that is much higher than the ERM working evaporating temperature T_e, and consequently have a vacuum in evaporator. As a result of this, it is necessary to have an additional device to evacuate air from the ejector system.

Comparative analysis shows that refrigerant R141b, which has the highest critical temperature, has the highest efficiency for a CCMC. The lowest efficiency occurs with refrigerant R236fa which has the lowest critical temperature. Other refrigerants have similar COP_{therm} values. Note that refrigerant R141b is toxic, and refrigerants R142b and R123 do not meet modern environmental requirements. Refrigerant R245ca also can be considered as a prospective working fluid for ERMs, but only for higher evaporating temperatures in the evaporator, for instance, in cascade refrigeration machines, where the ERM acts as the topping cycle.

The obtained results (Fig. 6a) also demonstrate convincingly that the application of a CCMC under the same operating conditions causes performance improvement up to 23.6% in comparison to ejectors with a CMC. The lowest improvement was observed for refrigerants R142b and R600a. The enhancements for refrigerant R142b were only 0.7% and 1.5% in ω and COP_{therm}, respectively; and for refrigerant R600a, it is a little higher: 0.8% and 1.7% in ω and COP_{therm}, respectively. The maximum growth of the same performance characteristics reached 22.7% and 23.6% for R245ca. Further to this, the improvement in COP_{mech} for each refrigerant was the same as improvement in ω.

Comparative analysis confirmed that the environmentally friendly natural low-pressure hydrocarbons butane (R600) and isobutane (R600a) and working fluid R245fa offer the best performance combination. Refrigerant R245fa also has good thermodynamic properties, reasonable working pressures, and a high critical temperature, which makes it a useful candidate for an ejector cooling cycle. In addition, it is non-corrosive, non-toxic, and non-flammable, which makes its application nonhazardous without additional safety measures. For these reasons, we have selected refrigerant R245fa as the most suitable working fluid for general purpose applications in the present study.

6. Conclusions

Theoretical analysis of ejector design and ejector refrigeration cycle performance was carried out. Analysis showed that the performance characteristics of ejectors and the ejector refrigeration cycle depend strongly on the operating conditions, the efficiency of the ejector used, and the thermodynamic properties of the refrigerant used.

Reliable performance of the ejector system substantially depends on the reliability of feed pump operation, which is the critical component in the ejector cycle. This electrically actuated pump is the only element in the heat-driven ERM that has moving parts, and it therefore determines the operational safety, leak resistance and lifetime of the whole system.

We propose an improved 1-D model for the prediction of the entrainment ratio ω, and an optimal design for ejectors with a CMC and a CCMC.

Comparative analysis of the performance characteristics of eight low-pressure refrigerants confirms that the environmentally friendly hydrocarbons butane (R600) and isobutane (R600a) and working fluid R245fa offer the best performance combinations. Refrigerant R245fa was selected as the most suitable working fluid for general purpose applications in the present study.

Acknowledgments

This publication is based on the work supported by Award No.KUK-C1-014-12, made by King Abdullah University of Science and Technology (KAUST), Saudi Arabia.

REFERENCES

Boumaraf, L., Lallemand, A., 2009. Modeling of an ejector refrigerating system operating in dimensioning and off-dimensioning conditions with the working fluids R142b and R600a. Appl. Therm. Eng. 29, 265–274.

Cizungu, K., Mani, A., Groll, M., 2001. Performance comparison of vapour jet refrigeration system with environment friendly working fluids. Appl. Therm. Eng. 21, 585–598.

Eames, I.W., Ablwaifa, A.E., Petrenko, V.O., 2007. Results of an experimental study of an advanced jet-pump refrigerator operating with R245fa. Appl. Therm. Eng. 27, 2833–2840.

Granryd, E., 2001. Hydrocarbons as refrigerants – an overview. Int. J. Refrigeration 24, 15–24.

Guangming, C., Xiaoxiao, X., Shuang, L., Lixia, L., Liming, T., 2010. An experimental and theoretical study of a CO_2 ejector. Int. J. Refrigeration 33, 915–921.

Huang, B.J., Chang, J.M., Wang, C.P., Petrenko, V.O., 1999. A 1-D analysis of ejector performance. Int. J. Refrigeration 22 (5), 354–364.

Huang, B.J., Jiang, C.B., Hu, F.L., 1985. Ejector performance characteristics and design analysis of jet refrigeration system. J. Eng. Gas Turb. Power 107, 792–802.

Huang, B.J., Liu, R.H., Wu, J.H., Yen, J.W., Hsu, H.Y., Chang, J.M., 2010a. Field test of solar-assisted cooling system. In: Proc. EuroSun 2010 (Graz, Austria).

Huang, B.J., Yen, C.W., Wu, J.H., Liu, J.H., Hsu, H.Y., Petrenko, V.O., Chang, J.M., Lu, C.W., 2010b. Optimal control and performance test of solar-assisted cooling system. Appl. Therm. Eng. 30, 2243–2252.

Mazur, V., 2003. Optimum refrigerant selection for low-temperature engineering. Low Temp. Cryog. Refrig. 101–118.

Munday, J.T., Bagster, D.F., 1977. A new ejector theory applied to steam jet refrigeration. Ind. Eng. Chem. Process Des. Dev. 16, 442–449.

Nehdi, E., Kairouani, L., Elakhdar, M., 2008. A solar ejector air conditioning system using environment-friendly working fluids. Int. J. Energ. Res. 32, 1194–1201.

Petrenko, V.O., 1978. Investigation of Ejector Cooling Machine Operating with Refrigerant R142b. Odessa Technological Institute of Refrigeration Industry, Ukraine. Ph.D. thesis.

Petrenko, V.O., 2001. Principle of working fluid selection for ejector refrigerating systems. Refrig. Eng. Technol. 1 (70), 16–21.

Petrenko, V.O., 2009. Application of innovative ejector chillers and air conditioners operating with low-boiling refrigerants in trigeneration systems. In: Proc. Eurotherm Seminar No.85 September 7–9. Louvain-la-Neuve, Belgium.

Petrenko, V.O., Chumak, I.G., Volovyk, O.S., 2005a. Comparative analysis of the performance characteristics of an ejector refrigerating machine utilizing various low-boiling working fluids. Refrig. Eng. Technol. 5 (97), 25–35.

Petrenko, V.O., Volovyk, O.S., Ierin, V.O., 2005b. Areas of effective application of ejector refrigeration machines using low-boiling refrigerants. Refrig. Eng. Technol. 1 (93), 17–30.

Pridasawas, W., Lundqvist, P., 2007. A year-round dynamic simulation of solar-driven ejector refrigeration system with iso-butane as a refrigerant. Int. J. Refrigeration 30, 840–850.

Roman, R., Hernandez, J.I., 2009. Performance of ejector cooling systems using hydrocarbon refrigerants. In: Proc. Eurotherm Seminar No.85 September 7–9, Louvain-la-Neuve, Belgium.

Roman, R., Hernandez, J.I., 2011. Performance of ejector cooling systems using low ecological impact refrigerants. Int. J. Refrigeration 34, 1707–1716.

Selvaraju, A., Mani, A., 2004. Analysis of an ejector with environment friendly refrigerants. Appl. Therm. Eng. 24, 827–838.

Selvaraju, A., Mani, A., 2006. Experimental investigation on R134a vapour ejector refrigeration system. Int. J. Refrigeration 29, 1160–1166.

Scott, D., Aidoun, Z., Bellache, O., Ouzzane, M., 2008. CFD simulations of a supersonic ejector for use in refrigeration applications. In: International Refrigeration and Air Conditioning Conference at Purdue.

Sokolov, E.Y., Zinger, N.M., 1989. Jet Devices. Energoatomizdat, Moscow, p. 352.

Sriveerakul, T., Aphornratana, S., Chunnanond, K., 2007a. Performance prediction of steam ejector using computational fluid dynamics: part 1. Validation of the CFD results. Int. J. Therm. Sci. 46, 812–822.

Sriveerakul, T., Aphornratana, S., Chunnanond, K., 2007b. Performance prediction of steam ejector using computational fluid dynamics: part 2. Flow structure of a steam ejector influenced by operating pressures and geometries. Int. J. Therm. Sci. 46, 823–833.

Sun, D.W., 1999. Comparative study of the performance of an ejector refrigeration cycle operating with various refrigerants. Energ. Convers. Manage. 40, 873–884.

Varga, S., Oliveira, A.C., Diaconu, B., 2009. Numerical assessment of steam ejector efficiencies using CFD. Int. J. Refrigeration 32, 1203–1211.